bitrary Shape (Program BLUNT)," AFWL-TR-70-16, July 1970 Air Force Weapons Lab. Kirtland AFB, New Mex.

[3] Jones, D.J. and South, J.C., Jr., "A Numerical Determination of the Bow Shock Wave in Transonic Axisymmetric Flow About Blunt Bodies," NAE LR-586, May 1975, National Research Council, Ottawa, Canada.

[4] Van Dyke, M.D. and Gordon, H.D. "Supersonic Flow Past a Family of Blunt Axisymmetric Bodies," TR R-1, Oct. 1958, NASA.

Comparison of a Two-Dimensional Shock Impingement Computation with Experiment

J.C. Tannehill* and T.L. Holst†
Iowa State University, Ames, Iowa
J.V. Rakich‡
NASA Ames Research Center, Moffett Field, Calif.
and
J.W. Keyes§
NASA Langley Research Center, Hampton, Va.

Nomenclature

C = smoothing constant
M = Mach number
p = pressure
Pr = Prandtl number
q = heat flux
Re_D = Reynolds number based on diameter
T = temperature
β = stretching factor
γ = specific heat ratio
θ = angle measured from stagnation streamline (without impingement)

Subscripts

stag = stagnation point value (without impingement)
w = wall value
∞ = freestream value

In Ref. 1, two-dimensional, viscous, blunt-body flowfields with an impinging shock wave were computed using a time-dependent, finite-difference method to solve the complete set of Navier-Stokes equations. These computations were qualitatively compared with existing three-dimensional experiments because of the lack of suitable two-dimensional experiments. Recently, J.W. Keyes completed a series of two-dimensional tests in the Langley 20-in. Hypersonic Tunnel. In these tests, a planar shock wave was allowed to impinge on the cylindrical leading edge of a fin (shock parallel with centerline of leading edge) resulting in Type III and Type IV interference patterns.[2] The computational method described in Ref. 1 was used to compute numerically one of the Type IV flowfields. This Note compares the results of this computation with the experiment. In addition, recent numerical experiments showing the effects of grid size and numerical smoothing are presented to better establish the accuracy of the code.

Received November 3, 1975; revision received January 5, 1976. The computational work in this paper was supported by NASA Ames Research Center under Grant NGR 16-002-038 and the Engineering Research Institute, Iowa State University, Ames, Iowa.

Index category: Supersonic and Hypersonic Flow.

*Associate Professor, Department of Aerospace Engineering and Engineering Research Institute. Member AIAA.

†Research Associate, Department of Aerospace Engineering and Engineering Research Institute; now Aerospace Engineer, Analytical Fluid Mechanics Section, High-Speed Aerodynamics Division, NASA Langley Research Center. Member AIAA.

‡Research Scientist. Associate Fellow AIAA.

§Aerospace Engineer, Applied Fluid Mechanics Section, High-Speed Aerodynamics Division.

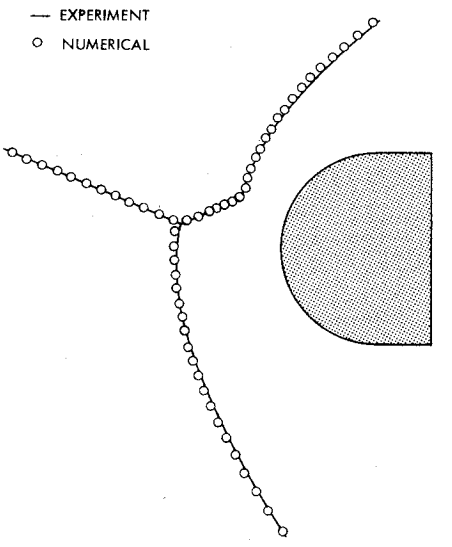

Fig. 1 Comparison of shock shapes.

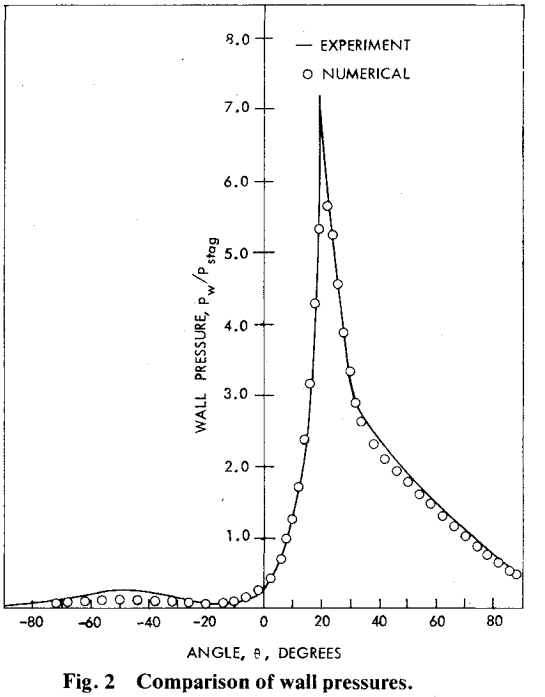

Fig. 2 Comparison of wall pressures.

The conditions of the test case were $M_\infty = 5.94$, $Re_{D_\infty} = 186{,}000$, $Pr = 0.72$, $p_\infty = 536$ N/m^2, $T_\infty = 59.5$ K, and $\gamma = 1.4$ with a leading edge radius of 0.0127 m and a wall temperature of 408 K. The impinging shock was inclined to the freestream at an angle of 22.75° and intersected the bow shock at $\theta = 7°$. Because of the much higher Reynolds number in this case, as compared to the Reynolds number in the cases of Ref. 1, it was necessary to use substantially more grid points. A grid composed of 81 points around the body ($\theta = -72°$ to $\theta = 88°$) and 61 points normal to it was employed in the final numerical computation. The mesh was refined near the body using a stretching factor (β) equal to 1.025. For this value of β, the first grid point off the body is located at 0.19% of the shock standoff distance as compared with 1.67% for no stretching.

A comparison between the numerical and experimental shock shapes is shown in Fig. 1. Excellent agreement is achieved. A comparison between the numerical and experimental wall pressures is shown in Fig. 2. Again, the com-

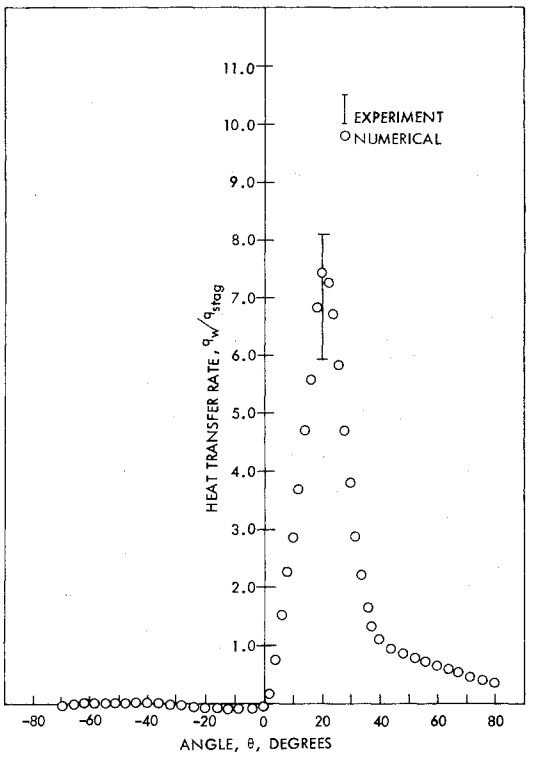

Fig. 3 Comparison of surface heat transfer rates.

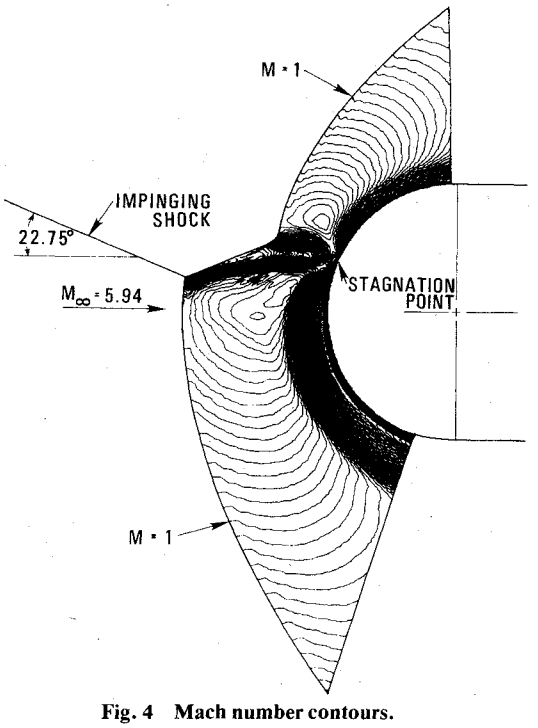

Fig. 4 Mach number contours.

parison is quite good although the numerical peak pressure is slightly less than the experimental peak pressure. The variation of the computed heat transfer rate around the body is shown in Fig. 3. The computed peak heat transfer rate is about 7.9 times the no-impingement stagnation point value. This value falls within the uncertainty range of the experiment. The Mach number contours for this case are shown in Fig. 4. These contour lines were drawn by a computer plotter in increments (ΔM) of 0.05 starting at $M=0$. The effects of the jet are clearly visible in this contour plot. Note that the slight oscillations which were present in Fig. 12 of Ref. 1 have

Table 1 Computational cases

Case	NJ	NK	C	β	$(\Delta z)_{min}$
1	31	51	0.50	1.080	0.0088
2	31	51	0.25	1.080	0.0088
3	51	81	0.25	1.050	0.0038
4	51	81	0.15	1.050	0.0038
5	61	81	0.15	1.025	0.0019

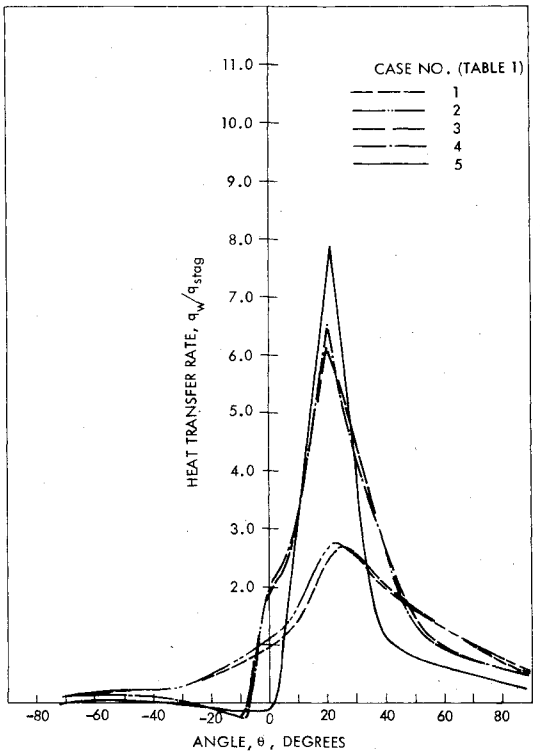

Fig. 5 Effects of smoothing and grid refinement.

been eliminated in this contour plot by applying MacCormack's smoothing scheme[3] over the entire mesh.

To determine the overall effects of smoothing and grid size on the computation, a comparison is made in Fig. 5 showing the heat transfer rates resulting from using different constants (C) in front of the smoothing term as well as using different computational grids. The different cases are described in Table 1 where NJ and NK represent the number of grid points normal to and around the body, respectively, and $(\Delta z)_{min}$ is the minimum grid spacing normal to the wall. The five cases in Table 1 were computed in a sequential fashion. That is, the results from Case 1 were used as the initial conditions for Case 2, etc. It is apparent from Fig. 5 that the effect of smoothing on the heat transfer rates is relatively small, whereas the effect of grid refinement is quite substantial. The peak heat transfer rate is not well predicted with 31 grid points between the body and the shock. A much better estimate is obtained with 51 or 61 grid points. It is felt that additional refinement in the radial direction would not improve the solution, although more refinement in the circumferential direction may be needed near the interaction region. On the other hand, it was found that neither smoothing nor grid refinement produced any significant changes in the wall pressures. Reasonable wall pressures (except for the peak values) were obtained with the 31×51 mesh.

References

[1] Tannehill, J.C., Holst, T.L., and Rakich, J.V., "Numerical Computation of Two-Dimensional Viscous Blunt Body Flows with an Impinging Shock," *AIAA Journal*, Vol. 14, Feb. 1976, pp. 204-211.

[2]Edney, B.E., "Anomalous Heat Transfer and Pressure Distributions on Blunt Bodies at Hypersonic Speeds in the Presence of an Impinging Shock," FFA Rept. 115, February 1968, The Aeronautical Research Institute of Sweden, Stockholm, Sweden.

[3]MacCormack, R.W., and Baldwin, B.S., "A Numerical Method for Solving the Navier-Stokes Equations with Application to Shock-Boundary Layer Interactions," AIAA Paper 75-1, Pasadena, California, 1975.

Airfoil Response to an Incompressible Skewed Gust of Small Spanwise Wave-Number

R. K. Amiet*
United Technologies Research Center, East Hartford, Conn.

Nomenclature

b = semichord
C_p = pressure coefficient
$f(M)$ = defined by Eq. (4)
$g(\xi)$ = defined by Eq. (7)
k_x = $\omega b/U$
k_y = $2\pi\, b$/spanwise gust wavelength
L = lift normalized by $2\pi\rho_0 U w_g b e^{i(\omega t - k_{y0} y)}$
Ω = Mach number of freestream
P = pressure
S = Sears function
t = time
U = freestream velocity
w_g = gust upwash
x,y = chordwise and spanwise coordinates normalized by b
β^2 = $1-M^2$
σ = $Mk_x/\beta k_y$
ω = circular frequency

Subscripts

0 = quantity related to incompressible skewed gust problem
∞ = quantity related to compressible parallel gust problem

Introduction

THE present Note derives an approximate solution for the response function of an infinite span airfoil in a three-dimensional (the gust wave fronts skewed relative to the airfoil leading edge) gust convecting with the freestream incompressible flow. The solution is limited to small spanwise wave number k_y. Together with the large k_y solution[1] (see also Ref. 2), the entire range of k_y can be observed. The present solution is derived from the parallel compressible gust result of Amiet,[3] using the similarity results of Graham.[4]

For the problem of an airfoil in a gust convecting with the freestream, Graham[4] related the general case of a skewed gust in compressible flow to either of the simpler cases of a parallel gust in compressible flow or a skewed gust in incompressible flow. If the parameter $\sigma \equiv Mk_x/\beta k_y \geq 1$, the similarity is to the parallel compressible gust case, whereas, if $\sigma \leq 1$, the similarity is to the skewed incompressible gust case. Thus, the solution for the parallel compressible gust case can be used throughout the regime $\sigma \geq 1$, and the skewed incompressible gust solution can be used in the regime $\sigma \leq 1$.

It was pointed out by Graham,[4] although it does not appear to be known widely, that each of these similarity rules can be used outside the regime for which it primarily is applicable. Thus, the solution for the case $\sigma < 1$ can be generated from the solution for $\sigma > 1$, and in particular, the result for a skewed incompressible gust ($\sigma = 0$) can be derived. The similarity rule used in the present note to relate the skewed incompressible gust case to the parallel compressible gust case was derived first by Graham, who gives further discussion and proof of the rule.[4]

Other approximate solutions to the problem of an airfoil encountering an incompressible skewed gust have been presented.[5,6] That of Ref. 5 is also a small k_y solution, although the order of accuracy was not given. The approximate two-dimensional compressible solution used as the base for the present solution was shown by Amiet,[3] and formally proven by Kemp and Homicz,[7] to be accurate to $O(Mk_x/\beta^2)$. From this, the skewed gust result presented herein is shown to be accurate to $O(k_y)$. Reference 6 gives an approximate solution which can be applied to all k_y. However, the present small k_y solution, together with the large k_y solution given in Refs. 1 and 2, gives significantly improved accuracy.

Result

The solution given by Graham[4] for the relation between the pressure coefficients C_p for the skewed incompressible gust case (subscript 0) and the parallel compressible gust case (subscript ∞) is

$$C_{p0}(x,k_{x0},k_{y0}) = \beta_\infty C_{p\infty}(x,k_{x\infty},M_\infty) \times \exp(-ik_{x\infty}M_\infty^2 x/\beta_\infty^2 - ik_{y0}y) \tag{1}$$

where

$$k_{x0} = k_{x\infty}/\beta_\infty^2 \qquad k_{y0}/k_{x0} = i\,M_\infty \tag{2}$$

In order to find the response to an incompressible skewed gust with small k_{y0}, the solution of Amiet[3] for the case of a low-frequency parallel compressible gust will be utilized. This solution has for the airfoil surface pressure,

$$P_\infty(x,t,k_{x\infty},M_\infty) = \mp(\rho_0 U w_g/\beta_\infty) \times [(1-x)/(1+x)]^{1/2} S(k_{x\infty}/\beta_\infty^2) \exp(i\{\omega t + k_{x\infty}[xM_\infty^2 + f(M_\infty)]/\beta_\infty^2\}) \tag{3}$$

where

$$f(M_\infty) = (1-\beta_\infty)\ln M_\infty + \beta_\infty \ln(1+\beta_\infty) - \ln 2 \tag{4}$$

and S is the classical Sears function. The minus or plus sign refers to the upper and lower airfoil surfaces, respectively. On substitution of Eqs. (3) and (4) into Eq. (1) and replacing the ∞ variables, using Eqs. (2), the airfoil surface pressure produced by a gust of the form

$$w_g(x,y,t) = w_g \exp[i(\omega t - k_{x0}x - k_{y0}y)] \tag{5}$$

in incompressible flow is found to be

$$P_0(x,y,t,k_{x0},k_{y0}) = P_\infty(x,t,k_{x0},0) \times \exp[ik_{x0}g(k_{y0}/k_{x0}) - ik_{y0}y] \tag{6}$$

where

$$g(\xi) = [(1+\xi^2)^{1/2} - 1]\,[i(\pi/2) - \ln\xi)] + (1+\xi^2)^{1/2}\ln[1+(1+\xi^2)^{1/2}] - \ln 2 \tag{7}$$

Received Dec. 1, 1975; revision received Jan. 15, 1976. The author would like to thank Professor J.M.R. Graham for additional values, not given in Ref. 8, for use in Table 1.

Index categories: Nonsteady Aerodynamics; Aircraft Gust Loading and Wind Shear.

*Senior Research Engineer. Member AIAA.